On the continuity of quantifying floating algae of the Central West Atlantic between MODIS and VIIRS

Mengqiu Wang & Chuanmin Hu

Taylor & Francis
Taylor & Francis Group

Check for updates

On the continuity of quantifying floating algae of the Central West Atlantic between MODIS and VIIRS

Mengqiu Wang[a] and Chuanmin Hu[b]

[a]College of Marine Science, University of South Florida, St. Petersburg, FL, USA; [b]College of Marine Science, University of 11 South Florida, St. Petersburg, FL, USA

ABSTRACT

Studying abundance and distributions of floating macroalgae such as pelagic *Sargassum* calls for long-term continuous and consistent observations from multiple satellite sensors. Previous studies mainly relied on observations from the Moderate Resolution Imaging Spectroradiometer (MODIS) and the Medium Resolution Imaging Spectrometer (MERIS). As a follow-on sensor, the Visible Infrared Imager Radiometer Suite (VIIRS) also has the appropriate spectral bands to detect and quantify floating macroalgae. Based on previous works on MODIS, this study presents an improved procedure to extract floating algae pixels from VIIRS Alternative Floating Algae Index (AFAI) imagery, with image filtering used to suppress noise and adjusted thresholds used to mask sun glint, clouds, and cloud shadows. The overall extraction accuracy is about 85%. Simultaneous daily observations from MODIS and VIIRS over the Central West Atlantic (CWA) show consistent spatial patterns, but VIIRS estimations of the algae coverage (in km^2) are consistently lower than MODIS (around − 19% mean relative difference or MRD), possibly due to lower sensitivity of the VIIRS near-infrared (NIR) bands than the corresponding MODIS bands. Similarly, at monthly scale VIIRS also shows lower coverage than MODIS, and their difference (around − 29% MRD) is larger than the difference between MODIS-Aqua and MODIS-Terra estimates (around − 14% MRD). Despite these differences, the spatial and temporal patterns between VIIRS and MODIS observed algae distributions match very well at all spatial and temporal scales. These results suggest that VIIRS can provide continuous and consistent observations of floating algae distributions and abundance from MODIS as long as their differences are accounted for, thus assuring continuity in the future. Furthermore, once *Sargassum* biomass per unit *Sargassum* area is determined from field measurements, conversion of these area estimates to *Sargassum* biomass is straightforward.

1. Introduction

Floating macroalgae of pelagic *Sargassum* in the Central West Atlantic (CWA) have shown an increasing trend and drastic inter-annual variability in recent years (Gower and King 2011; Gower, Young, and King 2013; Wang and Hu 2016; Wang and Hu 2017).

During bloom seasons (spring and summer), massive *Sargassum* beaching events in the Caribbean countries have been frequently reported, which caused significant problems to local tourism, fishery, ecology, and environment (Hu et al. 2016; Webster and Linton 2013; Maurer, De Neef, and Stapleton 2015). Similarly, in other oceans, an increasing trend of other types of floating macroalgae has also been reported (Smetacek and Zingone 2013), such as *Ulva prolifera* (a type of green macroalgae) in the Yellow Sea (Qi et al. 2016; Hu, Hu, and He 2017). Synoptic and frequent observations from satellite ocean color sensors provide effective means to monitor, assess, and understand changes of floating macroalgae at large spatial and temporal scales.

Currently, remote detection of floating macroalgae mainly relies on the enhanced reflectance in the near-infrared (NIR) spectral bands (the vegetation 'red-edge') (Gower et al. 2006). The red-edge reflectance allows for the development and application of several indexes, including the Maximum Chlorophyll Index (MCI) for the Medium Resolution Imaging Spectrometer (MERIS; 2002–2012) and the Floating Algae Index (FAI) and Alternative FAI (AFAI) for the Moderate Resolution Imaging Spectroradiometer (MODIS; Terra: 2000-present, Aqua: 2002-present) (Gower et al. 2006; Hu 2009; Wang and Hu 2016). However, MERIS stopped functioning in 2012, and both MODIS sensors are aging with their designed 5 year mission life, calling for continuous observations from other similar sensors. The Visible Infrared Imager Radiometer Suite (VIIRS; 2011-present) on the Suomi National Polar-orbiting Partnership satellite is also equipped with spectral bands similar to those of MODIS, thus could be used to generate VIIRS AFAI images. Such images have been developed and used in the *Sargassum* Watch System (SaWS) for near real-time monitoring of floating macroalgae (Hu et al. 2016). With proper masking of clouds, cloud shadows, and sun glint, floating macroalgae appear as elongated slicks in the AFAI imagery, thus can be easily visualized even by a layperson (Wang and Hu 2016).

However, beyond near real-time monitoring, assessment of long-term trends requires accurate feature extraction and data-binning strategies as well as consistent data products from multiple sensors, including the most recent VIIRS. Gower and King (2011) made the first attempt to map and quantify *Sargassum* abundance using statistical analyses of MERIS images (Gower and King 2011; Gower, Young, and King 2013), followed by a new mapping scheme developed for MODIS AFAI imagery (Wang and Hu 2016; 2017). However, to date although VIIRS AFAI imagery has already been used for visual inspection in the near real-time SaWS (Hu et al. 2016), automatic algae detection is still hindered by noise contamination (see Figure 1, Figure S1, and Figure S2) and false positive detection near clouds and cloud shadows. Furthermore, it is unclear whether VIIRS could provide consistent observations of algae distributions and abundance to continue the MODIS time series in case both MODIS instruments stop functioning, although such a continuity has been demonstrated for other ocean color data products such as water clarity (Barnes and Hu 2015). Therefore, the objectives of this study are:

- To develop an automatic algae extraction procedure to apply to VIIRS AFAI imagery;
- To compare VIIRS and MODIS performance on their ability to detect and quantify floating macroalgae using concurrent and collocated imagery;
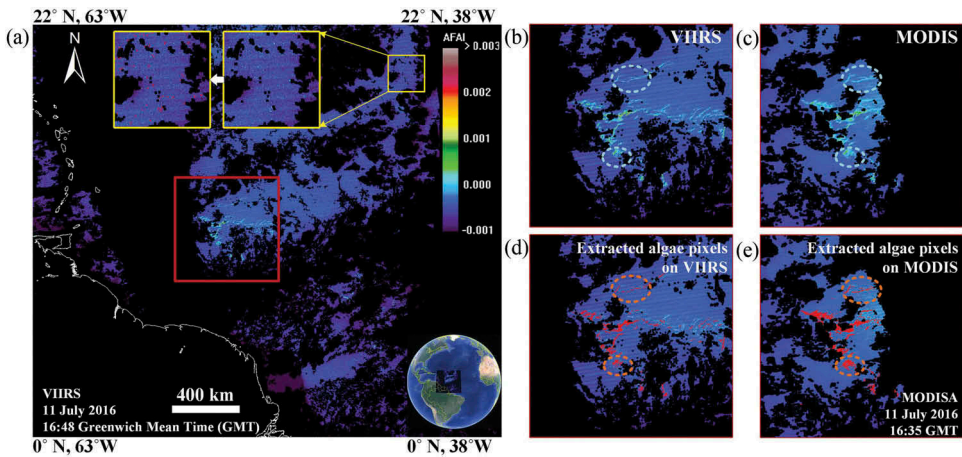
Figure 1. (*a*) A VIIRS AFAI image showing floating algae slicks outlined in the red box. The yellow boxes highlight the region with striping and other noise due to low SNRs (the brighter noise pixels are marked in red). (*b*) – (*c*): Quasi-simultaneous (within 30 minutes) VIIRS AFAI and MODIS AFAI images from the same locations outlined by the red box in (*a*). (*d*) – (*e*): Extracted algae pixels (marked in red) on VIIRS and MODIS AFAI images. Note that MODIS images also contain some level of striping artifacts although it is not obvious in this example. The dashed ellipses highlight that more algae pixels are detected in MODIS image than in VIIRS image. In regions where both sensors have valid observations, the number of algae pixels extracted from VIIRS is 2536, and 4568 from MODIS. Such a large difference is largely removed after a pixel unmixing scheme is applied to estimate algae coverage (in km^2).

- To quantify differences between VIIRS- and MODIS-derived long-term statistics in algae abundance and observing capacity.

2. Data and methods

MODIS and VIIRS Level-0 data for the entire year of 2016 with sufficient coverage (> 25%) over the CWA (0–22°N, 63–38°W) were obtained from the U.S. National Aeronautics and Space Administration (NASA) Goddard Space Flight Center (Ocean Color 2017), and processed to generate Rayleigh-corrected reflectance (R_{rc}) for each spectral band using the software package SeaWiFS Data Analysis System (SeaDAS) (version 7.2). Level-0 data instead of Level-1 data were used here because for a large region such as the CWA, multiple data granules may need to be merged together, and it is straightforward to merge Level-0 granules before processing. The R_{rc} data were then mapped at 1 km spatial resolution in the equidistant rectangular projection. A total of 1148 MODIS 5 minute granules (581 from MODIS-Aqua (MODISA) and 567 from MODIS-Terra (MODIST)) and 782 VIIRS 6 minute granules were downloaded and processed to R_{rc} data, which were then used to calculate AFAI for each pixel:

$$\text{AFAI} = R_{rc,NIR} - R'_{rc,NIR}$$

$$R'_{rc,NIR} = R_{rc,RED} + \left(R_{rc,LNIR} - R_{rc,RED}\right)(\lambda_{NIR} - \lambda_{RED})/(\lambda_{LNIR} - \lambda_{RED}) \quad (1)$$

The subscripts RED, NIR, and LNIR (long NIR wavelength) represent the corresponding spectral bands. For MODIS AFAI, λ_{RED} = 667nm, λ_{NIR} = 748nm, and λ_{LNIR} = 869nm. For VIIRS AFAI, three similar bands were used (λ_{RED} = 671nm, λ_{NIR} = 745nm, and λ_{LNIR} = 862nm). AFAI was chosen over the original FAI for better cloud masking performance (Wang and Hu 2016).

Figure 1 illustrates an example of VIIRS AFAI imagery showing floating algae pixels as bright features outlined in the red box. Compared to the quasi-simultaneous MODIS AFAI image, the VIIRS AFAI image shows more noise contamination due to lower signal-to-noise ratios (SNRs) of VIIRS. Such noise represent a major hurdle in automatic algae extraction. Therefore, noise reduction should be a critical preprocessing step to reduce false positive detection. After noise reduction, algae extraction from VIIRS AFAI imagery can follow the same workflow as that applied to MODIS AFAI imagery, including cloud and cloud shadow masking and removal of background variations (Wang and Hu 2016). Similar to MODIS processing, such a workflow was realized through a two-step procedure based on 4th order polynomial surface fitting and median filtering (Wang and Hu 2016). The thresholds for cloud and cloud shadow masking, however, were adjusted specifically for VIIRS (see Section 2.2).

2.1. *Noise reduction*

There are two types of noise in the VIIRS AFAI imagery. One is the striping artifacts due to imperfect detector calibration and different radiometric responses of the detectors of the whiskbroom scanner (Cao et al. 2014). To facilitate algae extraction, a recently developed destriping algorithm (Mikelsons et al. 2014) was tested on the VIIRS AFAI imagery (before map projection), with performance demonstrated in Figure S1. In most regions, the destriping algorithm effectively reduced the striping artifacts. However, some algae slicks aligned in parallel to the striping artifacts were also attenuated because they were treated as noise. On the other hand, although these stripes are noticeable in the VIIRS AFAI imagery, algae signals are often stronger and therefore can be well discriminated in both visual interpretation and threshold-based segmentation. Based on these considerations, destriping was not applied to VIIRS AFAI imagery.

The other type of noise often shows up near the scan edge (see Figure 1(a) and Figure S2). Unlike striping artifacts, these noise pixels are brighter than the nearby water pixels, thus must be removed to minimize false positive detection. Here, an 11 × 11 Gaussian filter was applied to the AFAI imagery to reduce such noise contamination. Several commonly used noise reduction methods were tested and compared in Figure S2. Among those, Gaussian filtering shows satisfactory performance as it can preserve most real features while reducing noise. However, because image filtering inevitably attenuates signals, algae extraction results from the filtered imagery were only used to determine a location buffer where real features (i.e., algae pixels) were extracted from the original image within the buffer, thus avoiding the noise-induced false positive detection outside the buffer. The buffer was determined from an 11 × 11 pixel dilation over the extracted algae pixels from the Gaussian filtered imagery. The workflow of the extraction process is summarized in Figure S3. The window size of 11 × 11 pixels used in the filtering was a compromise between reducing false positive detection and stabilizing false negative detection (Figure S4). Although signal

attenuation can still occur, the final estimates of algae coverages are not strongly affected because most algae features are still detectable and feature extraction is conducted over the original images. This procedure proves to be effective in preserving true algae pixels while reducing false positives (Figure S2).

2.2. Selection of thresholds to mask sun glint, clouds, and cloud shadows and to extract algae pixels

In the presence of sun glint, clouds, or cloud shadows, no information can be retrieved from the contaminated pixels, and these pixels were masked and treated as no observations. Because both sun glint and clouds have higher reflectance than nearby water in all spectra bands, these pixels were masked using a set of criteria as defined in Equation (2). This threshold-based masking method is the same as that used for MODIS AFAI imagery (Wang and Hu 2016), but with updated thresholds determined through trials and errors.

$$R_{rc}(671) \geq 0.05, \ or \ R_{rc}(745) \geq 0.05, \ or \ R_{rc}(862) \geq 0.05 \tag{2}$$

Although cloud shadow pixels show lower R_{rc} values than nearby water pixels in all spectral bands (Wang and 2016), the decreases in reflectance in different bands are not proportional, resulting in higher AFAI values than nearby water pixels, thus causing false positive detection. To mask these pixels, a local total R_{rc} (LTR), defined as the total R_{rc} in the 410 nm and 443 nm bands, was used:

$$LTR = R_{rc}(410) + R_{rc}(443) \tag{3}$$

Pixels with LTR lower than the reference values (REF_{LTR}) by a threshold T_c (see Equation (4)) were masked and treated as no observations. REF_{LTR} was calculated as the mean LTR of the surrounding 31 × 31 pixels.

$$LTR - REF_{LTR} < T_c \tag{4}$$

To better preserve the algae features while masking cloud shadow pixels, histograms of manually selected cloud shadow pixels and floating algae pixels were used to determine the cloud shadow threshold T_c (Figure 2(a,c)). T_c was determined to be −8.0 10^{-3}.

After correcting the large-scale gradient across the image, algae pixels were extracted using a global threshold T_0. Following the same steps as those applied to MODIS images (Wang and Hu 2016), T_0 was determined to be 2.0 10^{-4}. As demonstrated in Figure 2(b, d), over 96.0% of the adjacent water pixels are excluded while about 88.0% of the algae pixels are preserved after the global extraction threshold was applied.

2.3. Algae pixel unmixing

In nature, floating algae can rarely occupy the entire 1 km pixel (i.e., 100.0% coverage). A linear unmixing scheme was used to quantify the fractional coverage within each pixel through a global upper bound (representing 100.0% algae coverage) and a global lower bound (representing 0.0% algae coverage).

The lower bound was inferred from the nearby water pixels adjacent to the floating algae features, estimated to be − 4.4 10^{-4}. The upper bound was determined from field-
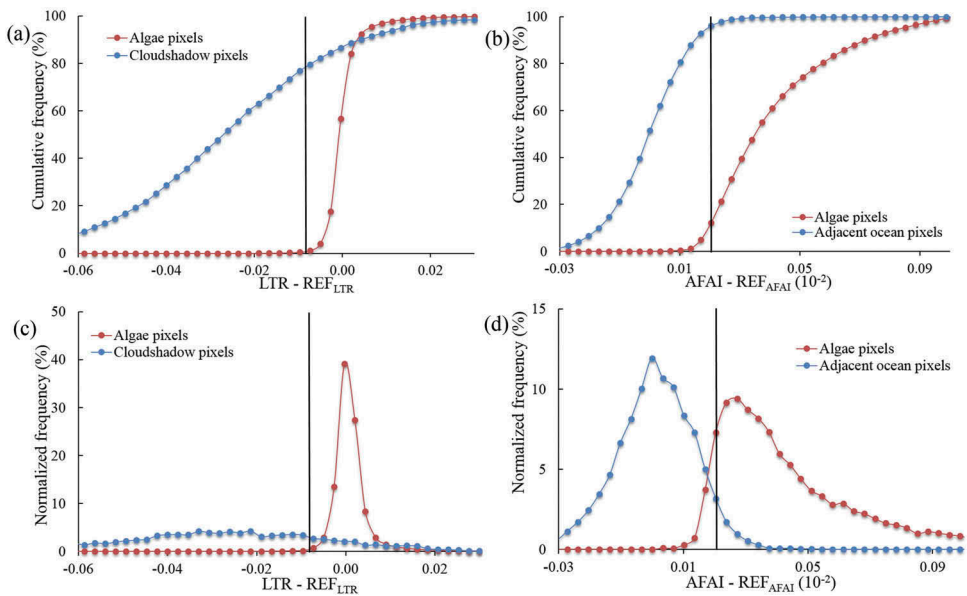
Figure 2. Cumulative and normalized frequency distributions of algae pixels, cloud shadow pixels, and adjacent ocean pixels in several regions of interest. (*a*) and (*c*) show the distributions of the (LTR − REF$_{LTR}$) values of algae pixels and cloud shadow pixels. (*b*) and (*d*) show the distributions of the (AFAI − REF$_{AFAI}$) values of algae pixels and adjacent ocean pixels. The adjacent pixels were selected by dilating 5 pixels into the nearest algae-free pixels.

measured *Sargassum* reflectance after propagating to top-of-atmosphere using radiative transfer simulations (Wang and Hu 2016). The simulations applied the relative spectral response (RSR) of VIIRS to field hyperspectral data, with the upper bound determined to be 4.6 10^{-2} (see Table S1 for details).

After linear unmixing of the extracted algae pixels with the selected upper and lower bounds, algae coverage maps were obtained, where pixels were assigned a value of 0.0% for algae-free water pixels and between 0.0% and 100.0% for algae-containing pixels. Pixels with no observations due to clouds, cloud shadows, land, land adjacent area, sun glint, or no satellite coverage were all masked as invalid values.

2.4. *Cross-sensor comparisons*

VIIRS and MODIS data products were compared at different time scales, from snapshot imagery to composite imagery. Following Wang and Hu (2016), the entire study region was divided into 0.5° × 0.5° grids, where fractional algae coverage from the original high-resolution images was aggregated into each grid to obtain mean algae density (% cover) for a given time interval (month, season, or year). The seasons were defined as boreal meteorological seasons. In the comparisons, unless Aqua or Terra is explicitly stated, the term 'MODIS' represents the combined observations from both Aqua and Terra.

The cross-sensor difference was assessed using the mean relative difference (MRD) (Barnes and Hu 2015) between the two measurements:

$$\text{MRD} = \frac{1}{N}\sum_{i=1}^{N}\frac{y_i - x_i}{x_i}100\% \tag{5}$$

where y_i and x_i stand for the measurement of algae coverage or number of valid observations. The comparison was conducted between MODIS (individual sensors or combined) and VIIRS where x_i represents the measurements from MODIS, and also between the individual MODIS sensors (MODIST and MODISA) where x_i represents the measurements from MODISA.

To evaluate whether differences in algae coverage statistics might be due to differences in the number of valid observations, the daily percentage valid observations (DPVOs) (Feng and Hu 2016) at any 1 km location from a given 0.5° grid was calculated as:

$$\text{DPVO} = \frac{N_v}{3025\ d}\ 100\% \tag{6}$$

where N_v is the number of valid 1 km observations in each grid during a time interval and d is the number of days during the time interval, while $55 \times 55 = 3025$ is maximum possible valid observations in the same grid from a given day (0.5°Corresponds to about 55 1 km pixels). For example, a DPVO of 15.0% indicates that the probability of having a valid observation at any 1 km location within the grid in a given day in that time interval is 15.0%.

3. Results

3.1. *Algae extraction accuracy*

Accurate extraction of algae-containing pixels is a prerequisite for long-term statistical analyses. To evaluate the extraction performance, 12 representative VIIRS AFAI images (6 from February and 6 from August 2016) were selected. The 'ground-truth' data of true algae pixels were selected using an the Interactive Data Language (IDL) graphical user interface (GUI) designed to extract image features with morphological constraints guided by visual interpretations (Wang and Hu 2015). Results from the accuracy assessments are summarized in Table 1. For the area coverage estimated using unweighted algae pixels, false positive and false negative rates (Chinchor and Sundheim 1993) are 28.9% and 19.6%, respectively. After weighting each pixel using the fractional (percentage) coverage, both rates are reduced significantly, with an overall extraction accuracy of 85.5%, comparable to the algae extraction accuracy from MODIS (Wang and Hu 2016). The reason why a better extraction accuracy was obtained after weighting each algae-

Table 1. Accuracy assessment of delineation of algae-containing pixels from 12 VIIRS AFAI images in February and August 2016.

	False positive (%)	False negative (%)	Precision (%)	Recall (%)	F score (%)
Area coverage using unweighted algae pixels (AUP)	28.9	19.6	73.6	80.4	76.8
Area coverage using weighted algae pixels (AWP)	13.4	10.6	86.3	84.6	85.5

containing pixel (for its fractional coverage) is because the false-detection (both false positive and false negative) pixels generally have lower weights (fractional coverages) than those of the correctly extracted ones. For example, a pixel with 10.0% algae coverage is counted for 1.0 if weighting is not applied, but counted for 0.1 if weighting is applied. This suggests that the proposed algae extraction procedure for VIIRS is at least as accurate as that for MODIS, thus allowing for the comparison of VIIRS and MODIS on their capacity for quantifying algae coverage at both image level and long-term scales.

3.2. *Comparison of quasi-simultaneous observations between MODIS and VIIRS*

Before comparing algae coverage statistics derived from MODIS and VIIRS, it is important to understand whether they lead to the same algae coverages for simultaneous observations. To address this question, 98 image pairs of quasi-simultaneous measurements (within 30 minutes) in 2016 were selected. It is assumed that within 30 minutes algae features do not move or change significantly, thus allowing for a direct comparison. For the same reason, the comparison was performed from the common pixels where both MODIS and VIIRS showed valid observations.

   Although there is a relatively large discrepancy between MODIS- and VIIRS-derived number of algae pixels (Figure 3(a)), after pixel weighting they show consistent algae coverages (Figure 3(b)). This is because that many of the undetected pixels in the VIIRS imagery have low weights (i.e., low sub-pixel fractional coverages), thus having relatively small effects on the area estimates. Linear regression between MODIS- and VIIRS-derived algae area coverages in Figure 3(b) shows a significant positive relationship (the coefficient of determination (R^2) = 0.95; F = 1211.1; $p \ll 0.001$). The slope of the linear regression is 0.94, suggesting that their coverage estimates only differ by a few percent for most images. The negative intercept (–2.27 km^2) (i.e., VIIRS is generally lower than MODIS) may be a result of undetected weak algae slicks in VIIRS AFAI imagery (Figure 1).

   Two outlier clusters that depart from the main trend are worth mentioning here. One is for pixels that are marked as algae on VIIRS but not on MODIS AFAI imagery (blue
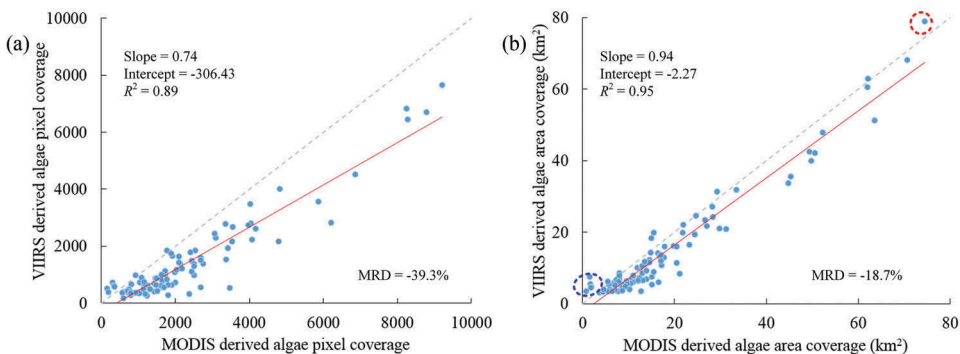

Figure 3. Quasi-simultaneous MODIS and VIIRS measurements over the same observed pixels in the CWA showing numbers of derived algae pixels in (*a*) and algae area coverages in (*b*). The dashed lines are the 1:1 reference lines and the red solid lines are the linear regression lines. The outliers marked in the blue and red circles are explained in the text.

dashed circle in Figure 3(b)). Visual inspection shows that this is due to false positive detection from residual cloud shadow pixels in the VIIRS imagery. The other is for pixels showing higher algae coverage from VIIRS than from MODIS (red dashed circle in Figure 3(b)). Visual inspection shows that this is due to the low detectability on the scan edge, where many algae features visible in the VIIRS imagery are located on the MODIS scan edge, thus too weak to be detected in the MODIS AFAI imagery. Nevertheless, the comparison shows a MRD of − 18.7% in the algae area estimates between MODIS and VIIRS, indicating relative consistency and compatibility between the two datasets. The lower algae detectability from VIIRS imagery is possibly due to its lower SNRs than MODIS, but it would not significantly impact the long-term statistics of algae coverage.

3.3. *Comparison of long-term statistics*

Because pixels near scan edge may be missed in algae extraction, they were masked before statistical calculations. Pixels with satellite view zenith angle (VZA) > 60° were regarded as having no observations and excluded from the calculations. The VZA of 60° is the standard threshold used in the Level-2 processing to flag data with large viewing angles, and pixels with VZA above this threshold are not used in the global composites of data products (Patt et al. 2003). The fraction of the observations meeting this masking criterion is 10.6% for MODIS and 29.3% for VIIRS in 2016.

Overall, statistics of mean area coverages from MODIS and VIIRS long-term measurements show larger differences than from quasi-simultaneous images, with lower coverages derived from VIIRS. The difference was quantified with the MRD between the total area coverage (in km^2) for each time interval. The MRD was determined to be − 28.7%, − 30.4%, and − 24.9% for monthly, seasonal, and annual mean coverages between the two measurements. While detailed comparison results for monthly and seasonal mean algae coverages are summarized in Figure S5, Table S2, and Table S3, Figure 4 compares monthly mean algae coverage from MODISA, MODIST, MODIS (i.e., MODISA and MODIST combined), and VIIRS measurements, all showing significant positive correlations. MODIST shows lower estimations than MODISA but higher estimations than VIIRS. The MRD between MODIST and VIIRS measurements (−23.4%) is lower than that between the two MODIS measurements (−14.1%).

The difference between VIIRS and MODIS estimates appears to come from an offset of 30–50 km^2. Therefore, in summer months where algae coverage is much higher than in winter months, the relative difference can be much smaller. For example: in December 2016, VIIRS-derived algae coverage is only 33.0% of the MODIS estimate, but in July 2016 VIIRS shows 89.0% of the MODIS estimate (Figure 4(a), Table S2). Likewise, annual mean coverage in 2016 derived from VIIRS is 132 km^2 or about 75.0% of the MODIS estimate (176 km^2).

The monthly and seasonal mean algae distribution maps are provided in Figure S6 and Figure 5, respectively. Although the algae abundance (in area intensity) derived from VIIRS is consistently lower than that from MODIS, the spatial patterns and their temporal variations are similar. Blooms first appear in the tropical Atlantic in spring, and are then transported to the Caribbean Sea in summer following the prevailing winds and currents (Wang and Hu 2017).
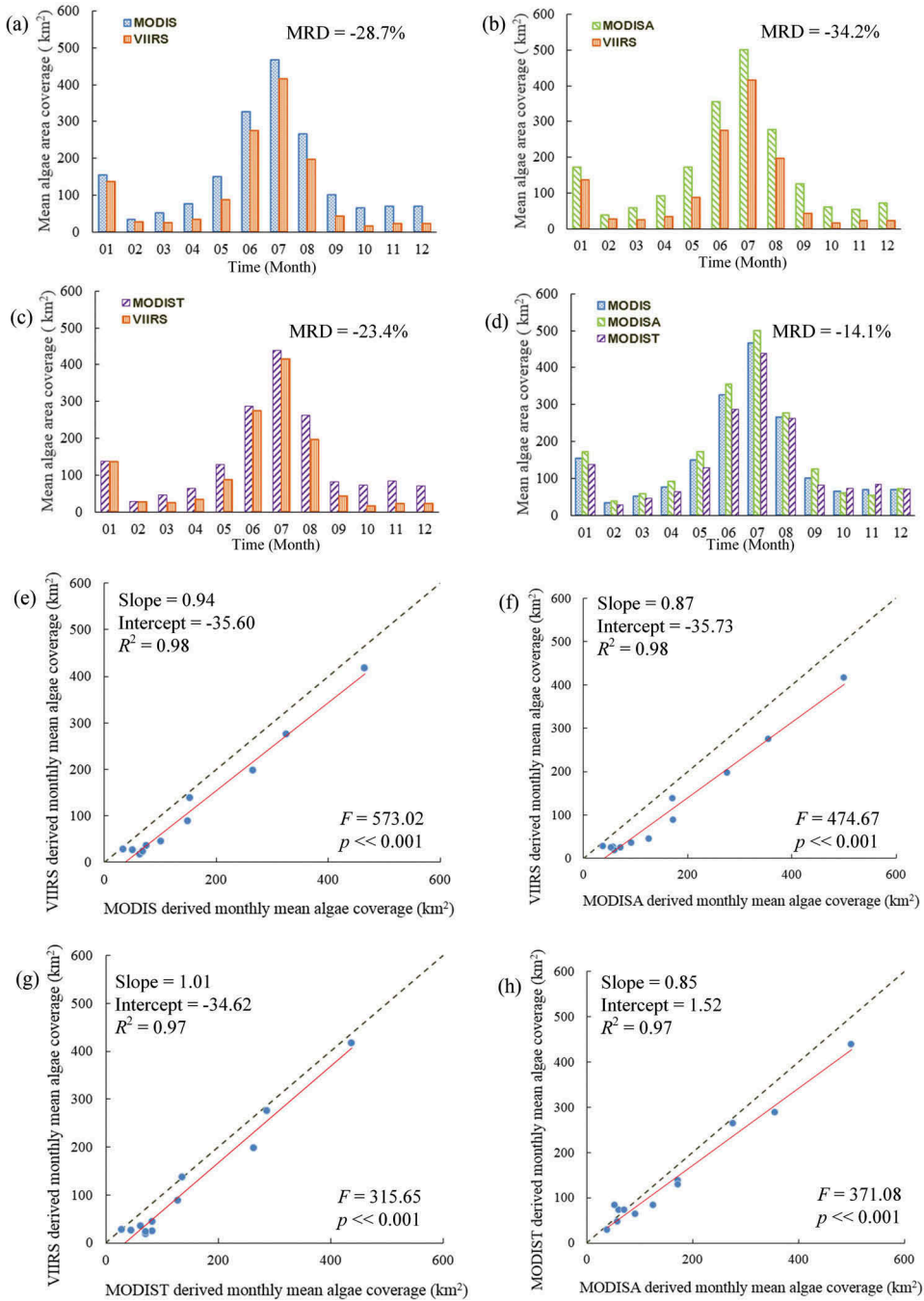
Figure 4. (*a*) – (*d*): Monthly mean algae coverage over the CWA during 2016 determined from MODIST, MODISA, MODIS (i.e., MODIST and MODISA combined), and VIIRS. The MRD marked on (*d*) is between MODISA and MODIST. (*e*) – (*h*): Linear fit of the monthly mean algae coverages from different measurements. The dashed lines are the 1:1 reference lines and the red solid lines are the linear regression lines.
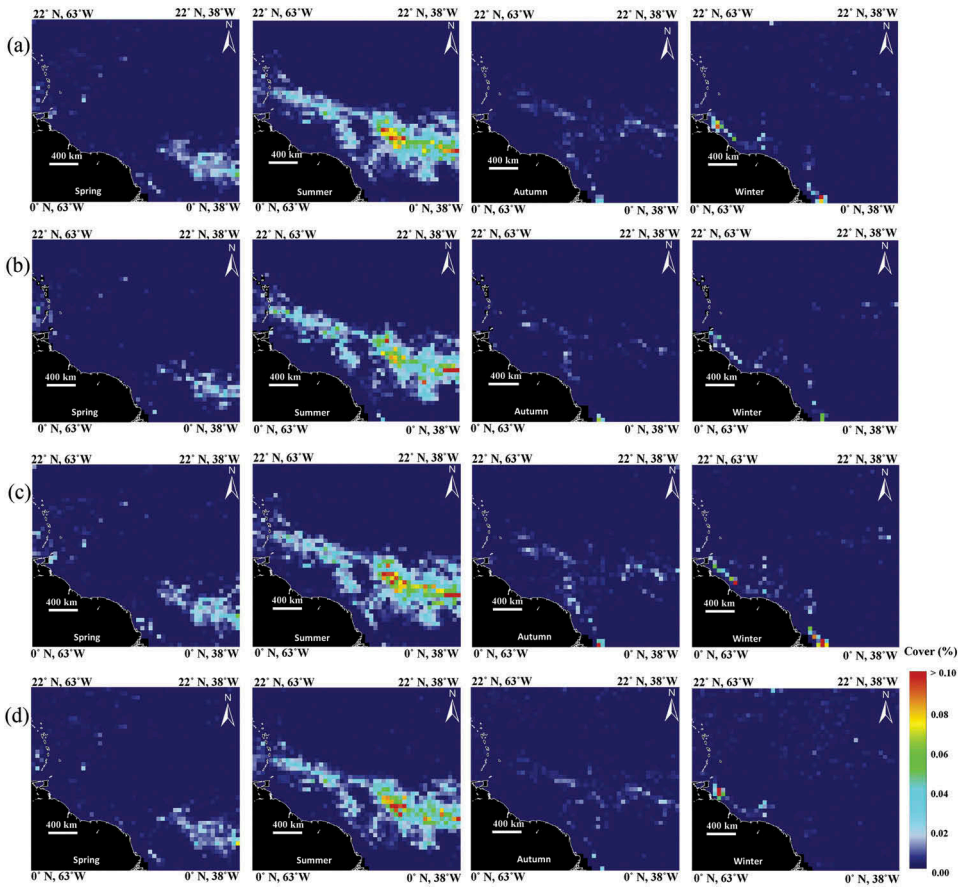
Figure 5. Seasonal mean algae area coverages in 2016 derived from MODIS (*a*), VIIRS (*b*), MODISA (*c*), and MODIST (*d*). Land and coastlines are masked in black and white, respectively. The color indicates % algae coverage in each 0.5° × 0.5° grid.

These results from monthly, seasonal, and annual statistics suggest that VIIRS can provide estimates consistent to those from MODIS in both the spatial patterns and temporal variations. Furthermore, after applying the corresponding scaling and offset factors based on the relationships derived in Figure 4 and Figure S5, VIIRS observations may provide a consistent time series in the future to continue the MODIS observations, assuring cross-sensor continuity.

4. Discussions

In this study as well as in Wang and Hu (2016), *Sargassum* abundance is estimated as area density (% cover) in each grid cell and area coverage (km^2) for the study region. Once biomass per *Sargassum* area is determined from field measurements, conversion of these estimates to biomass per grid cell or total biomass for the area is straightforward. For example, assuming 2 kg *Sargassum* wet biomass per m^2 (Mizuno et al. 2014), a 0.1% area density corresponds to 2 g m^{-2} wet biomass or 2000 kg km^{-2} biomass. Such

determined biomass per area or total biomass in a specific region will provide critical information to understand the potential environmental and ecological impacts and to guide management efforts. The question is what are the uncertainties in these estimates.

In addition to the algae extraction procedure itself, several inherent factors of the satellite sensors may lead to various uncertainties in the extraction results and in the area estimates. These factors include sensor SNRs, pixel spatial resolutions, and data availability.

4.1. *Sensor SNRs*

Using simulations and *Sargassum* spectra measured in the field, Hu et al. (2015) estimated that for a 200:1 SNR in the NIR wavelengths, the lower detection limit of sub-pixel algae coverage is about 1.0% of the pixel size (Hu et al. 2015). This simulation result is indirectly confirmed by MODIS statistics in Wang and Hu (2016), where the lower detection limit is about 0.2% of the MODIS pixel size because MODIS SNRs in the NIR wavelengths are about 1000:1 (Hu et al. 2012), 5 times of the SNRs used in the simulation. SNRs of VIIRS NIR bands under typical radiance inputs of ocean environments have not been reported, but our unpublished data using the same SNR estimation procedure indicate that VIIRS SNRs in the NIR bands are about 500:1 regardless of the aggregation zone along the scan direction. The lower SNRs of VIIRS thus may explain, at least partially, why VIIRS-based algae area estimates are generally lower than those from MODIS (Figures 3 and 4).

4.2. *Pixel resolution*

Once SNRs are fixed, the lower detection limit of sub-pixel algae coverage in terms of % pixel size is also fixed. Then, the lower detection limit in terms of algae area (in km^2) is proportional to pixel size, which always increases from scan center to scan edge for a polar-orbiting scanner such as MODIS and VIIRS.

For MODIS, Figure S7 (*a*) suggests that pixel size increases rapidly after VZA > 45° (basically a cosine effect, about 6 times on scan edge over scan center). For VIIRS, the pixel growth rate is much constrained by aggregating sequential detector read-outs and the pixel size is approximately 2 times on scan edge over scan center (Schueler, Lee, and Miller 2013). To determine the impact of pixel size (or the spatial sampling size) on algae area estimates, we compared the percent of undetected *Sargassum* coverage using VIIRS-detected *Sargassum* in 2016, with results summarized in Table S4.

With a SNR of 1000:1 for MODIS, the detection limit is 0.2% of pixel size according to image statistics (Wang and Hu 2016). Then, for pixels near scan center, the detection limit is about 0.002 km^2. For pixels near scan edge (VZA > 55°), the detection limit is 0.012 km^2.

For this change of pixel size from scan center to scan edge, if all detected *Sargassum* in 2016 were put in pixels near scan edge, 44.4% of detected *Sargassum* would be undetected. However, only 11.0% of satellite data are located near scan edge (VZA > 55°), so in reality only 11.0% × 44.4% = 4.9% of all *Sargassum* will be undetected (last row of Table S4). Likewise, only 32.7% × 0.9% = 0.3% of all *Sargassum* will be undetected from

pixels between scan center and scan edge. For VIIRS, these numbers will be even smaller because near scan edge VIIRS pixel size is much smaller than MODIS.

Clearly, although pixel size impacts the detectability (i.e., larger pixel size leads to higher detection limit in terms of km^2) of *Sargassum* within a pixel, the impacts on the overall area estimates are rather small (about 5.0%), lower than the uncertainties from the algae extraction procedure itself (around 14.5%, see Table 1). The impacts on VIIRS (from scan center to scan edge) are smaller than on MODIS, and they are both within the 5.0% uncertainty bounds, thus making negligible differences when cross-sensor consistency is the goal for observing continuity.

4.3. *Data availability and valid observations*

In addition to sensor sensitivity and pixel size, statistics of algae coverage can also be affected by data availability or number of valid observations. Insufficient number of valid observations could lead to statistical biases. For an extreme example, if during a month there is only one valid observation in the study region, if this observation is an algae pixel then the algae coverage is assumed to be 100.0% for the entire region in that month. Likewise, if this observation is an algae-free water pixel, then the algae coverage is assumed to be 0.0% for the entire region in that month. Obviously, neither is realistic due to lack of valid observations. To assess whether some of the differences in the algae statistics could be due to differences in their data availability, seasonal maps of DPVOs for MODIS and VIIRS are compared in Figure 6, and the area-averaged DPVOs are summarized in Figure 7.

During all seasons of 2016, a combination of MODISA and MODIST (i.e., MODIS) shows more valid observations than VIIRS or individual MODIS sensors, especially in the north of the CWA region. At lower latitudes, both MODIS and VIIRS show fewer valid observations due to frequent and persistent cloud cover near the Inter-tropical Convergence Zone (ITCZ) (Wylie et al. 2005). As shown in Figure 6, more valid observations are found in the summer and autumn for both MODIS and VIIRS. The mean area-averaged DPVOs is 20.8% for MODIS and 11.5% for VIIRS. Such a data availability (around 10.0%) from any single sensor (either MODIST, MODISA, or VIIRS) doubles that for global ocean chlorophyll observations from MODISA or MODIST (about 5.0%, Feng and Hu 2016) despite the fact that the study region is in the ITCZ. This is obviously due to the different requirements on data quality, as MODIS global composites have more stringent requirements on data quality. MODIST shows more valid observations than MODISA in all months (Feng and Hu 2016), but fewer valid observations than VIIRS. While the former is possibly due to more sun glint in MODISA than in MODIST images, the latter is a result of larger swath width of VIIRS (3050 km) than MODIS (2330 km). When all three sensors are combined, the maximum observing capacity is obtained. In any case, a combination of two or more sensors leads to significantly more valid observations than any single sensor, arguing for more instruments from polar-orbiting satellites or more measurements from, for example, a geostationary platform. This is not only important for reducing potential aliasing in statistics, but also critical for near real-time applications that require data availability every day (Hu et al. 2016).
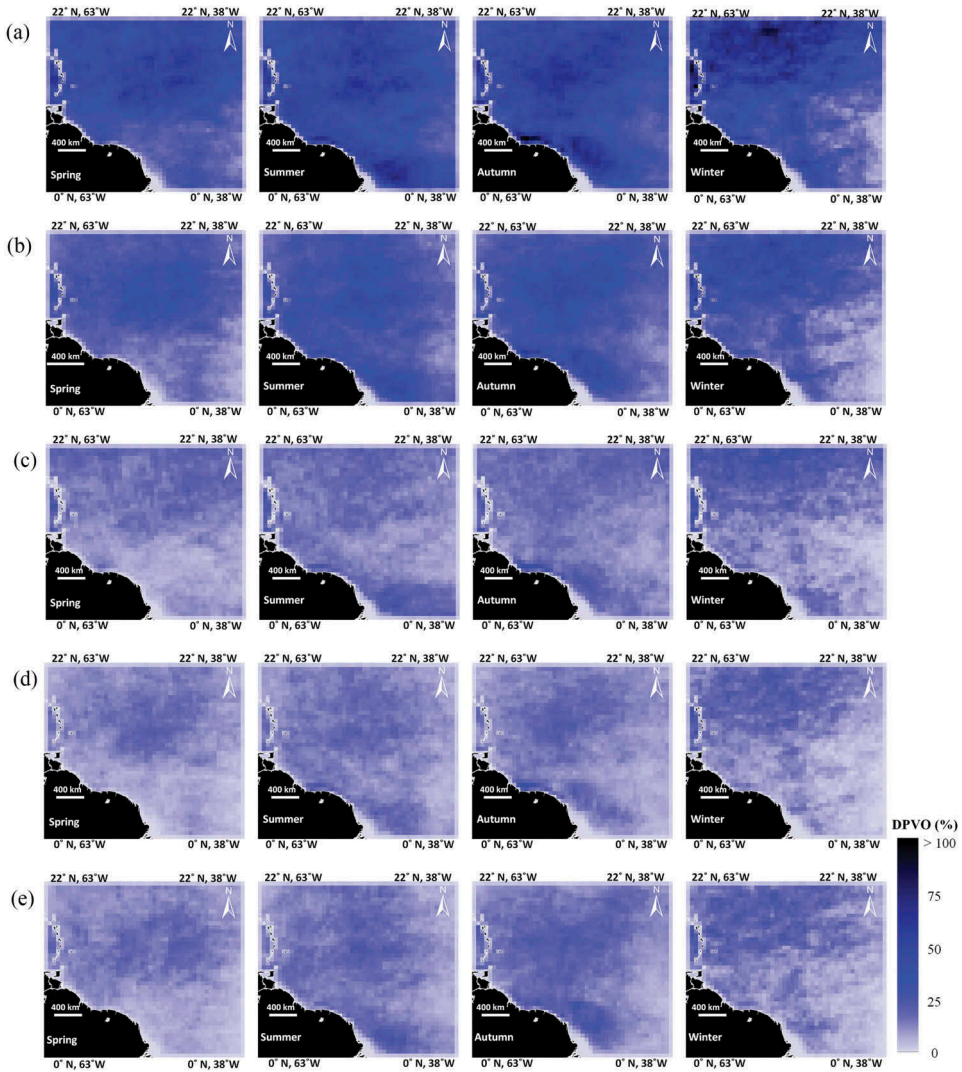
Figure 6. Comparison of DPVOs between MODIS and VIIRS in each season of 2016. (*b*), (*c*), (*d*), and (*e*) show the DPVOs from MODIS, VIIRS, MODISA, and MODIST, respectively. (*a*) lists the DPVOs from both MODIS and VIIRS. The regions near land (dilated 20 km outward from shoreline) are masked to avoid perturbations of the shallow-water bottom. A number of 25 in the color legend means that there is a 25% chance of obtaining valid observations at a given 1 km location in a given day.

4.4. *Validation*

Direct validation of the estimated *Sargassum* area coverage is extremely difficult or even impossible for several reasons. One, the coarse satellite pixels (about 1 km) will always miss small *Sargassum* mats, as shown in Hu et al. (2015) using satellite and airborne images with different resolutions (1 km, 30 m, 8 m, and centimetres). This has also been shown by the contrasting results from Gower and King (2011) and from Hardy (2014) where the former did not report any *Sargassum* in the eastern Gulf of Mexico through
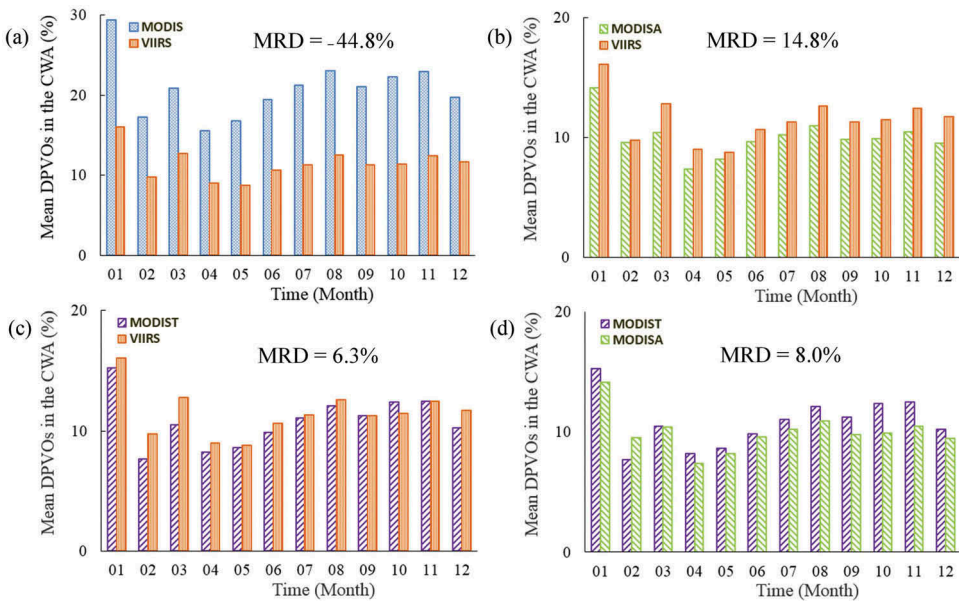
Figure 7. Comparison of area-averaged DPVOs in each month of 2016 between different sensors. The mean DPVOs of MODIS, VIIRS, MODISA, and MODIST are 20.82%, 11.49%, 10.01%, and 10.81%, respectively. The MRDs between different sensors are annotated in the figures.

analyzing 1 km MERIS data but the latter showed large amounts through analyzing 30 m Landsat data (Hardy 2014). The contrasting results are mainly due to their resolution difference. Two, *Sargassum* mats in the ocean move with currents and winds, making it difficult to correlate field and satellite observations in the same locations at the same time. However, as stated in Wang and Hu (2016) when using MODIS to map *Sargassum*, the results represent *Sargassum* observable by the specific satellite sensor under realistic ocean conditions. Therefore, considering that the focus of this paper is on the continuity of *Sargassum* observing, the emphasis is not the absolute amount but rather the consistency between MODIS and VIIRS. For this purpose, the validation is on the unmixing approach using finer-resolution images to provide the 'truth'.

For this type of validation, two pairs of MODISA and Landsat-8 (L8) images were analyzed with results provided in Figure S8. As expected, *Sargassum* slicks extracted from MODISA and L8 images show similar patterns, with L8 capturing more small features. On the other hand, the area estimates derived from MODISA and L8 for the same slicks are very close, suggesting the accuracy of the unmixing approach.

4.5. Implications for different applications

Overall, with reduced SNRs but slightly improved spatial resolution, VIIRS shows *Sargassum* detection accuracy of 85.5%, comparable to MODIS performance. The area estimates as well as spatial/temporal patterns are also consistent with those obtained from MODIS, although in general VIIRS shows lower area estimates primarily due to its lower SNRs in the NIR bands as opposed to different data availability (DPVOs) from

individual observations. The validity of the pixel unmixing results, as verified by comparisons of measurements from MODIS and Landsat, suggests that both SNRs and spatial resolution are key requirements for accurate detection and quantification of *Sargassum* mats.

There are several implications from these findings. First, operation of the near real-time SaWS requires as much data as possible from multiple sensors. This is because that the same locations that are not observable from one sensor (due to sun glint, clouds, cloud shadows, or large VZAs) may be observable from another. The validated performance of VIIRS makes such an addition in data quantity not only feasible, but with data quality comparable to that of MODIS. This is particularly useful when considering the wider swath width of VIIRS (3050 km) than MODIS (2330 km). Two, for science applications, VIIRS can serve as a continuity mission in case both MODIS sensors stop functioning, especially after adjusting their differences using regression equations derived from concurrent observations from all sensors. Likewise, because the recent Sentinel-3 Ocean and Land Color Instrument (OLCI) is also equipped with similar red and NIR bands as on MODIS and VIIRS, a similar continuity study may lead to consistent observations to those of MODIS and VIIRS as well. Finally, at the time of this writing, VIIRS-II on the Joint Polar Satellite System (JPSS) follow-on mission is planned to be in space by 2018, which is expected to provide consistent observations of floating algae from the MODIS and VIIRS time series, thus extending the current observations to the foreseeable future.

5. Conclusion

VIIRS is equipped with similar red and NIR bands as MODIS, and VIIRS AFAI imagery have been created and used routinely in the near real-time SaWS for detecting and tracking floating macroalgae such as *Sargassum*. However, VIIRS has different SNRs, spatial resolutions, and swath width from MODIS. This study presents the first evaluation results of VIIRS capacity for detecting and quantifying *Sargassum* macroalgae, in reference against MODIS observations. Results suggest that the inclusion of VIIRS data can not only increase data quantity with similar data quality of MODIS, but also provide continuous and consistent observations of spatial/temporal patterns of *Sargassum* macroalgae should MODIS sensors stop functioning.

Acknowledgments

Disclosure statement

No potential conflict of interest was reported by the authors.

References

Barnes, B. B., and C. Hun. 2015. "Cross-Sensor Continuity of Satellite-Derived Water Clarity in the Gulf of Mexico: Insights into Temporal Aliasing and Implications for Long-Term Water Clarity Assessment." *IEEE Transactions on Geoscience and Remote Sensing* 53 (4): 1761–1772. doi:10.1109/TGRS.2014.2348713.

Cao, C., F. J. De Luccia, X. Xiong, R. Wolfe, and F. Weng. 2014. "Early On-Orbit Performance of the Visible Infrared Imaging Radiometer Suite Onboard the Suomi National Polar-Orbiting Partnership (S-NPP) Satellite." *IEEE Transactions on Geoscience and Remote Sensing* 52 (2): 1142–1156. doi:10.1109/TGRS.2013.2247768.

Chinchor, N., and B. Sundheim. 1993. MUC-5 Evaluation Metrics. Paper presented at the Proceedings of the 5th conference on Message understanding.

Feng, L., and C. Hu. 2016. "Comparison of Valid Ocean Observations between MODIS Terra and Aqua over the Global Oceans." *IEEE Transactions on Geoscience and Remote Sensing* 54 (3): 1575–1585. doi:10.1109/TGRS.2015.2483500.

Gower, J. F. R., and S. A. King. 2011. "Distribution of Floating *Sargassum* in the Gulf of Mexico and the Atlantic Ocean Mapped Using MERIS." *International Journal of Remote Sensing* 32 (7): 1917–1929. doi:10.1080/01431161003639660.

Gower, J., C. Hu, G. Borstad, and S. King. 2006. "Ocean Color Satellites Show Extensive Lines of Floating *Sargassum* in the Gulf of Mexico." *IEEE Transactions on Geoscience and Remote Sensing* 44 (12): 3619–3625. doi:10.1109/TGRS.2006.882258.

Gower, J., E. Young, and S. King. 2013. "Satellite Images Suggest a New *Sargassum* Source Region in 2011." *Remote Sensing Letters* 4 (8): 764–773. doi:10.1080/2150704X.2013.796433.

Hardy, R. F. 2014. "Assessments of Surface-Pelagic Drift Communities and Behavior of Early Juvenile Sea Turtles in the Northern Gulf of Mexico." MA thesis, University of South Florida (Publication No. 1569947).

Hu, C., B. Murch, B. B. Barnes, M. Wang, J. P. Maréchal, J. Franks, D. Johnson, B. E. Lapointe, D. Goodwin, and J. Schell. 2016. "*Sargassum* Watch Warns of Incoming Seaweed." *EOS Transactions American Geophys Union* 97 (22): 10–15. doi:10.1029/2016EO058355.

Hu, C. 2009. "A Novel Ocean Color Index to Detect Floating Algae in the Global Oceans." *Remote Sensing of Environment* 113 (10): 2118–2129. doi:10.1016/j.rse.2009.05.012.

Hu, C., L. Feng, R. F. Hardy, and E. J. Hochberg. 2015. "Spectral and Spatial Requirements of Remote Measurements of Pelagic *Sargassum* Macroalgae." *Remote Sensing of Environment* 167: 229–246. doi:10.1016/j.rse.2015.05.022.

Hu, C., L. Feng, Z. Lee, C. O. Davis, A. Mannino, C. R. McClain, and B. A. Franz. 2012. "Dynamic Range and Sensitivity Requirements of Satellite Ocean Color Sensors: Learning from the Past." *Applied Optics* 51 (25): 6045–6062. doi:10.1364/AO.51.006045.

Hu, L., C. Hu, and M. X. He. 2017. "Remote Estimation of Biomass of *Ulva Prolifera* Macroalgae in the Yellow Sea." *Remote Sensing of Environment* 192: 217–227. doi:10.1016/j.rse.2017.01.037.

Maurer, A. S., E. De Neef, and S. Stapleton. 2015. "*Sargassum* Accumulation May Spell Trouble for Nesting Sea Turtles." *Frontiers in Ecology and the Environment* 13 (7): 394–395. doi:10.1890/1540-9295-13.7.394.

Mikelsons, K., M. Wang, L. Jiang, and M. Bouali. 2014. "Destriping Algorithm for Improved Satellite-Derived Ocean Color Product Imagery." *Optics Express* 22 (23): 28058–28070. doi:10.1364/OE.22.028058.

Mizuno, S., T. Ajisaka, S. Lahbib, Y. Kokubu, M. N. Alabsi, and T. Komatsu. 2014. "Spatial Distributions of Floating Seaweeds in the East China Sea from Late Winter to Early Spring." *Journal of Applied Phycology* 26 (2): 1159–1167. doi:10.1007/s10811-013-0139-8.

Ocean Color. 2017. National Aeronautics and Space Administration Goddard Space Flight Center. Accessed March 20 2017. http://oceancolor.gsfc.nasa.gov

Patt, F. S., R. A. Barnes, R. E. Eplee Jr, B. A. Franz, W. D. Robinson, G. C. Feldman, and S. W. Bailey. 2003. "Algorithm Updates for the Fourth SeaWiFS Data reprocessing,NASA Tech. Memo. 2003–206892." In *SeaWiFS PostlaunchTechnical Report Series*, edited by S. B. Hooker and E. R. Firestone, 74. Vol. 22. Greenbelt, Maryland: NASA Goddard Space Flight Center.

Qi, L., C. Hu, Q. Xing, and S. Shang. 2016. "Long-Term Trend of *Ulva Prolifera* Blooms in the Western Yellow Sea." *Harmful Algae* 58: 35–44. doi:10.1016/j.hal.2016.07.004.

Schueler, C. F., T. F. Lee, and S. D. Miller. 2013. "VIIRS Constant Spatial-Resolution Advantages." *International Journal of Remote Sensing* 34 (16): 5761–5777. doi:10.1080/01431161.2013.796102.

Smetacek, V., and A. Zingone. 2013. "Green and Golden Seaweed Tides on the Rise." *Nature* 504 (7478): 84–88. doi:10.1038/nature12860.

Wang, M., and C. Hu. 2015. "Extracting Oil Slick Features from VIIRS Nighttime Imagery Using a Gaussian Filter and Morphological Constraints." *Ieee Geoscience and Remote Sensing Letters* 12 (10): 2051–2055. doi:10.1109/LGRS.2015.2444871.

Wang, M., and C. Hu. 2016. "Mapping and Quantifying *Sargassum* Distribution and Coverage in the Central West Atlantic Using MODIS Observations." *Remote Sensing of Environment* 183: 350–367. doi:10.1016/j.rse.2016.04.019.

Wang, M., and C. Hu. 2017. "Predicting *Sargassum* Blooms in the Caribbean Sea from MODIS Observations." *Geophysical Research Letters* 44 (7): 3265–3273. doi:10.1002/2017GL072932.

Webster, R. K., and T. Linton. 2013. "Development and Implementation of *Sargassum* Early Advisory System (SEAS)." *Shore & Beach* 81 (3): 1.

Wylie, D., D. L. Jackson, W. Paul Menzel, and J. J. Bates. 2005. "Trends in Global Cloud Cover in Two Decades of HIRS Observations." *Journal of Climate* 18 (15): 3021–3031. doi:10.1175/jcli3461.1.